

PARAMETER ESTIMATION IN X-RAY ASTRONOMY REVISITED

Tahir Yaqoob¹

Laboratory for High Energy Astrophysics, NASA / Goddard Space Flight Center,
Code 662, Greenbelt, MD 20771.

NOTE: This version supercedes all previous versions you may have seen. Substantially incorrect versions of this paper were sent out due to a departmental clerical error.

To appear in the Astrophysical Journal, June 20, 1998, vol. 499

Received _____; accepted 16 January 1998

¹ Also with the Universities Space Research Association.

ABSTRACT

The method of obtaining confidence intervals on a subset of the total number of parameters (p) of a model used for fitting X-ray spectra is to perturb the best-fitting model until, for each parameter, a range is found for which the change in the fit statistic is equal to some critical value. This critical value corresponds to the desired confidence level and is obtained from the χ^2 distribution for q degrees of freedom, where q is the number of interesting parameters. With the advent of better energy-resolution detectors, such as those onboard *ASCA* (*Advanced Satellite for Cosmology and Astrophysics*) it has become more common to fit complex models with narrow features, comparable to the instrumental energy resolution. To investigate whether this leads to significant non-Gaussian deviations between data and model, we use simulations based on *ASCA* data and we show that the method is still valid in such cases. We also investigate the weak-source limit as well as the case of obtaining upper limits on equivalent widths of weak emission lines and find that for all practical purposes the method gives the correct confidence ranges. However, upper limits on emission-line equivalent widths may be over-estimated in the extreme Poisson limit.

Subject headings: methods: data analysis – methods: statistical – X-rays: general

1. INTRODUCTION

The procedure for generating confidence intervals for the parameters of models used to fit X-ray spectra with the χ^2 minimization technique is well established (e.g. Lampton, Margon and Bower 1976; Avni 1976). One uses the fact that if χ_{true}^2 is the value of the statistic from a given experiment, calculated for the ‘true model’ (known only to nature) and χ_{min}^2 is the value of the statistic obtained from the best-fitting model, then from many repetitions of the same experiment $\Delta\chi^2 = \chi_{\text{true}}^2 - \chi_{\text{min}}^2$ has a probably distribution like χ^2 with p degrees of freedom ($\equiv \chi_p^2$) where p is the total number of free parameters. Confidence intervals generated for the p parameters from the χ_p^2 distribution are then *joint* confidence intervals for all p parameters. If we are interested only in a subset q of the p parameters then the confidence intervals are generated from the χ_q^2 distribution. The crucial difference between p -parameter and, say, one-parameter errors is as follows. In the former case the $P\%$ confidence intervals from χ_p^2 will *simultaneously* enclose the true values of all parameters in $P\%$ of all experiments. In the latter case, the $P\%$ intervals from χ_1^2 will enclose the true values of any of the parameters in $P\%$ of all experiments, *but it will be a different $P\%$ subset of experiments for each parameter*. In a particular case, the number of ‘interesting’ parameters (i.e. q) is determined by the scientific problem being posed.

In principle one generates the $\Delta\chi^2$ space by stepping through a q -dimensional grid of parameter values. The use of χ^2 in model-fitting requires that there are a sufficient number of photons per energy bin for the statistical variations to be Gaussian. However, with the advent of better energy resolution X-ray detectors it is increasingly becoming the case that the Gaussian approximation cannot be made unless the spectrum is binned, sacrificing valuable information. In such cases the statistical variation in counts per bin is Poisson and one must use the maximum likelihood ratio (hereafter, ‘ C statistic’) to optimize the model parameters (see Cash 1979). Cash (1979) demonstrated that the C statistic can be used

to generate confidence intervals in an analogous manner to χ^2 since ΔC has a probability distribution like χ^2 except for terms of order α/\sqrt{n} where α depends on the model and n is the number of photons carrying information about the parameter in question. Hereafter, we shall use C for the sake of generality.

Lampton *et al.* (1976) warned that (at that time), there was no general proof that the technique for projection of the subset of q parameters did not depend explicitly on model linearity. Then, Avni (1976), using some non-linear models in simulations of *Uhuru* data, showed that the χ_q^2 region worked in these particular cases, but there was still no general proof. Such a proof was presented by Cash (1976), showing that the χ_q^2 region worked for any data set, *provided that the deviations are Gaussian*. We must remember that X-ray detectors now have much better energy resolution and sensitivity than they did then and accordingly the models have become much more complex. Both Lampton *et al.* (1976) and Avni (1976) used *Uhuru* spectral responses with seven energy bins between 1 and 7 keV, and simple power-law or plasma models. It is not clear whether, for example, a model including a narrow emission line whose intrinsic width is comparable to the energy resolution of the detector, would introduce non-Gaussian deviations between model and data. The purpose of this paper is to check whether the method for parameter estimation currently in use gives the correct confidence intervals even with the new generation of improved energy-resolution instrumentation. We are particularly interested in models with features such as emission lines and absorption edges (which occur frequently in a wide range of X-ray sources), whose widths in energy space are comparable to the instrumental energy resolution. We also wish to check the Poisson regime, when the source count rate is low, and when upper limits must be obtained on the equivalent width of weak or non-detected emission-line features.

The structure of the paper is as follows: §2 describes basic simulations and models used in the investigation; §3 describes the basic results; §4 demonstrates the equivalence

of emission-line equivalent width and intensity confidence regions; §5 describes results for the extreme Poisson limit and §6 describes results pertaining to measuring upper limits on weak emission-line features. Our conclusions are stated in §7.

2. SIMULATIONS

We investigated the behavior of ΔC for various models by means of simulations of spectra from *ASCA* (Tanaka, Inoue and Holt 1994), using the spectral fitting code XSPEC (Shafer *et al.* 1989). The spectral response function for one of the ‘Solid-state Imaging Spectrometers’ aboard *ASCA* (SIS0) was used in the simulations. The simulated spectra consisted of 330 pulse height bins of width $\sim 0.03 - 0.3$ keV covering the energy range 0.5 – 10 keV. At 6 keV the energy resolution is $\sim 2\%$, or ~ 130 eV. No attempt was made to simulate the internal or sky background. In practice, if one is using the C statistic the background cannot be subtracted since C strictly requires Poisson statistics. The background must be modelled and the resulting model included together with the source model in the spectral fitting process, fixing the background model parameters, which therefore do not make any contribution to ΔC .

We used six different models, described in Table 1, where the exact parameter values are specified. In each case the basic continuum model is a power law plus absorption, typical of the X-ray spectra of active galactic nuclei (AGNs). The 2–10 keV flux corrected for absorption was $\sim 5 \times 10^{-11}$ ergs cm $^{-2}$ s $^{-1}$ and the exposure time was 40 Ks in each case (unless specified otherwise). This exposure time is typical for *ASCA* observations. For each model the following process was repeated 1000 times. A simulated spectrum was created and the value of the statistic recorded. This is just C_{true} , which characterizes the Poisson deviations of the data away from the true (i.e input) model. A spectral fit was then performed on the simulated data using the same model, with all the parameters free. The

best-fitting parameters were recorded, as well as the corresponding value of the statistic, C_{\min} . Next, each parameter, i , was fixed at its true (input) value and then C was minimized over the remaining parameters, giving a value, C_i , for each parameter. We then examined the probability distributions of $\Delta C_{\text{true}} \equiv C_{\text{true}} - C_{\min}$ and $\Delta C_i \equiv C_i - C_{\min}$, as well as the behavior of ΔC_{true} and ΔC_i as a function of the best-fitting parameter values. We did not always use the results of all 1000 simulations since the few cases in which any of the ΔC were negative were rejected since this indicated that a proper minimization had not been achieved.

3. BASIC RESULTS

Figures 1a–1f show the cumulative probability distributions of ΔC_{true} (stars) and the ΔC_i (symbols used for the different parameters are explained in the Figures). The solid lines show the theoretical χ^2 distributions for 1 to p degrees of freedom where p is the total number of free parameters. Model 1 is the ‘control’ case, consisting only of a simple power law plus absorption with no localized, or narrow, features. In this case, Figure 1a shows that ΔC_{true} is distributed like χ_3^2 as expected, since $p = 3$. Thus, for a given ΔC_{true} and corresponding percentage probability, P , the $P\%$ *joint* confidence intervals of all p parameters will be given by the range of parameters associated with all the simulations that have $\Delta C \leq \Delta C_{\text{true}}$. This is because ΔC_{true} is computed with p adjustable parameters and $P\%$ of *all* experiments have $\Delta C \leq \Delta C_{\text{true}}$. Figure 1a also shows that all the ΔC_i are correctly distributed as χ_1^2 . The ranges of parameters associated with these distributions correspond to confidence intervals for one interesting parameter. For a given ΔC_i and the corresponding percentage probability, P , we can say that in $P\%$ of all experiments, parameter i will lie in the range associated with all the simulations that have $\Delta C \leq \Delta C_i$, but the remaining $p - 1$ parameters need not *simultaneously* lie in their respective, similarly

computed, single-parameter confidence ranges, *in the same set of experiments*. We also repeated the model 1 simulations with (1) N_H increased by a factor of 20, to 10^{23} cm^{-2} , and (2) exposure time reduced by a factor of 10, and confirmed similar results.

The results for model 2, which includes a narrow Gaussian emission line at 6.4 keV (intrinsic width, $\sigma_{\text{Fe}} = 0.1 \text{ keV}$, equivalent width, $\text{EW} = 100 \text{ eV}$), are shown in Figure 1b. The energy resolution of the *ASCA* SIS at 6.4 keV is $\sim 150 \text{ eV}$ or so, and Figure 1b shows that ΔC_{true} and ΔC_i still follow the χ_6^2 and χ_1^2 distributions respectively, with excellent agreement.

Figure 1c shows the results (again, as expected) of simulations with the Fe K line equivalent width increased to 500 eV, the remaining parameters being unchanged (model 3). The relations between the parameter ranges associated with ΔC_{true} and ΔC_i for model 3 are shown in Figure 2. The crosses show the ΔC_i plotted against the best-fitting values of each of the six model parameters, including the power-law normalization. It can be seen that for each parameter the points are consistent with a single-valued parabolic function, as expected. Also plotted are the ΔC_{true} against the best-fitting parameter values (dots). It can be seen that the dots lie completely inside the parabolic curves. If one draws a horizontal line on each plot, corresponding to a $P\%$ confidence level for p parameters then all the dots below the horizontal line include $P\%$ of all simulations. Since the dots were computed with p adjustable parameters, the parameter ranges associated with the dots are associated with the $P\%$ *joint* confidence intervals. However, since the dots are bounded by the crosses, the $P\%$ *joint* confidence intervals can be computed from the *single-parameter* ΔC space by choosing the appropriate value of the critical ΔC . The latter is the standard practice used in actual spectral analysis programs like XSPEC.

In models 4 and 5 the intrinsic width of the emission line was 0.3 keV and 0.01 keV respectively, but the center energies and equivalent widths had the same values as in model

2. Thus models 4 and 5 test the cases when the emission line is broader or narrower than the instrumental energy resolution respectively, and Figures 1d and 1e show that the results agree well with the predicted curves even for the very narrow line.

Figure 1f (model 6, Table 1) shows results for a case in which the localized spectral feature is not an emission line but an absorption edge, at 0.8 keV with an optical depth at the edge energy of $\tau_0 = 0.2$. Above the edge the optical depth is $\tau = 0.2(E/0.8 \text{ keV})^{-3}$. Such edge features, due to the ionized Oxygen, have been found in several AGNs (e.g. see Nandra and Pounds 1992). Spectral fitting of the simulated data was performed with the edge energy fixed or else the fits would become unstable (the same can happen with real data). The ΔC_{true} and ΔC_i distributions follow $\Delta\chi_4^2$ and $\Delta\chi_1^2$ respectively, as expected.

4. CONFIDENCE INTERVALS FOR EMISSION-LINE EQUIVALENT WIDTH

In practice, when analysing real data with spectral-fitting programs such as XSPEC, there is a problem with obtaining the confidence regions of the equivalent width of emission lines. This is because the equivalent width depends on the normalization and shape of the underlying continuum, as well as the line intensity. Thus, the equivalent width cannot in general be included as one of the model parameters. A common practice is to obtain the confidence region for the line intensity and then simply scale this by the best-fitting value of the equivalent width, as computed from the best-fitting values of the continuum parameters. We can use the results of our simulations to assess the validity of this approximation. Figure 3 (solid line) shows the actual distribution in the equivalent width of the emission line from the model 3 simulations. The dotted line shows the distribution of the line intensity, simply scaled by a single number (in this case, the input equivalent width of 500 eV), for a direct comparison. The two distributions are virtually indistinguishable and we confirmed this

for the other emission-line models. Thus with real data, one can safely derive confidence regions for the equivalent width of an emission line by simply rescaling the confidence regions of the intensity of that line with the best-fitting equivalent width value.

5. VERY WEAK SOURCES

We repeated the model 2 simulations, reducing the exposure time to 4 Ks, so that the entire 0.5–10 keV spectrum had less than 4,500 counts. In this case, when spectral fitting the simulated spectra we fixed the emission-line energy and intrinsic width so that there were a total of only four free parameters. Exactly the same procedure would be followed with real data for weak sources since the fits cannot be easily constrained so that one is forced to consider the restricted investigation of finding the intensity and/or equivalent width of the line for a given center energy and intrinsic width, rather than the more general problem of trying to constrain all three parameters. The results are shown in Figure 4a which shows that ΔC_{true} and the ΔC_i are in good agreement with $\Delta\chi_4^2$ and $\Delta\chi_1^2$ respectively, as expected.

We then repeated the model 2 simulations again, reducing the exposure time further to 400 s (less than 450 counts in the entire spectrum, contained in 330 bins). The results are shown in Figure 4b which shows that small discrepancies are apparent between the predicted and measured distributions of ΔC_{true} and ΔC for the line intensity. In this case, the line-intensity distribution is peaked at zero due to many non-detections of the line since there are so few photons. This is illustrated in Figure 5 which shows the distribution of ΔC_i (crosses) and ΔC_{true} (dots) as a function of the best-fitting line intensity for three exposure times, 40 Ks, 4 Ks and 400 s (panels (a), (b), and (c) respectively). In each case the same four-parameter model was used. It is apparent that for the extreme Poisson limit of 400 s exposure time, the deviations between model and data are less than expected since the line

intensity has become a trivial parameter. In practice, there is not much cause for concern, since one would not normally try to even obtain upper limits on the line intensity from a spectrum with so few counts. The discrepancies between the predicted and observed ΔC distributions are not so bad for large ΔC , which corresponds to cases when the line is more significant. Thus, obtaining 90% confidence upper limits on the line intensity is still possible but upper limits for lower confidence levels are likely to be somewhat over-estimated.

6. UPPER LIMITS ON WEAK LINE-EMISSION

Our results so far show that for all practical purposes the χ_q^2 region gives the correct confidence range for the intensity or equivalent width of an emission line, when the ‘true’ equivalent width is as small as 100 eV. In cases when the line is not detected, correct upper limits on the equivalent width may be obtained provided there are enough counts in the spectrum. However, we now consider the situation in which the equivalent width of the line in the ‘true’ model is small or zero. We addressed this by generating simulated data with model 1 (i.e. *no emission line* in the model) and then fitting the simulated data with model 2 (i.e. *including an emission line*), with the intensity as the only free line-parameter (fixing the center energy and intrinsic width at 6.4 keV and 0.1 keV respectively). This case, corresponding to no emission line in the ‘true’ model, when compared with the model 2 simulations in §3, then gives information on models with weak line-emission (i.e. input equivalent width between 0 and 100 eV). The simulations were performed for exposure times of 40 Ks and 4 Ks. Results for the latter are shown in Figure 6. It can be seen that there is fair agreement between ΔC_{true} and $\Delta\chi_4^2$ and between the ΔC_i and $\Delta\chi_1^2$. However, there is a slight departure between the measured and predicted ΔC_i for the line intensity. In practice, this will result in a slight overestimate of the upper limits on the equivalent width of the line. For an exposure time of 40 Ks, simulations show an effect of similar

magnitude and for an exposure time of 400 s, the situation is similar to the extreme Poisson limit discussed in §5. Thus we conclude that upper limits on the line equivalent width or intensity may be over-estimated when the line is weak or absent in the ‘true’ model. However, the confidence regions are approximately correct for practical purposes.

7. CONCLUSIONS

We have verified that for all practical purposes, the method of generating confidence intervals for a subset, q , of p model parameters, using the χ_q^2 distribution can still be used even if the model has components which are narrow compared to the instrumental energy resolution (such as emission lines and absorption edges). We have also investigated the weak-source and weak emission-line limits and find the method to work, except for the extreme Poisson limit when there may be one or less total counts per energy bin. In this case, equivalent widths of emission lines may be somewhat over-estimated.

It must be remembered, however, that the χ_q^2 confidence ranges can say nothing of the *simultaneous* confidence ranges of the other $p - q$ parameters. For example, suppose one observes an active galaxy or X-ray binary and measures the magnitude of an X-ray reflection continuum component (due to Compton-thick scattering) and the equivalent width of an iron-K line and quotes, as is common practice, 90% confidence errors for one interesting parameter ($\Delta\chi^2 = 2.7$). Now, the relation between the iron-K line equivalent width and the strength of the reflection continuum can be predicted from a theoretical model, so one can determine whether the measured values are consistent with such a model, within the errors. However, one-parameter errors (as used, for example, in Zdziarski *et al.* 1996) are inappropriate since these confidence ranges are not simultaneous. One must use two-parameter errors in such a case.

Much of this work was done during an extended stay at the Institute of Space and Astronautical Science (ISAS), Japan, during the summer of 1993 and two weeks in November 1996. The author thanks everyone in the X-ray astronomy group at ISAS for their great hospitality. The author would also like to thank Peter Serlemitsos, Richard Mushotzky, Andy Fabian, and Andy Ptak for useful discussions, and Keith Arnaud for generally maintaining XSPEC and fixing bugs promptly. The author is very grateful to Dr. W. Cash for correcting some serious errors in an earlier version of the paper and is also indebted to an anonymous referee for making some extremely important points which led to a complete revision of the paper.

REFERENCES

- Avni, Y. 1976, *ApJ*, 210, 642
- Cash, W. 1976, *A&A*, 52, 307
- Cash, W. 1979, *ApJ*, 228, 939
- Lampton, M., Margon, B., & Bowyer, S. 1976, *ApJ*, 208, 177
- Nandra, K., & Pounds, K. A. 1992, *Nat*, 359, 215
- Shafer, R. A., Haberl, F., & Arnaud, K. A. 1989, *XSPEC: An X-ray Spectral Fitting Package (ESA TM-09)*
- Tanaka, Y., Inoue, H., & Holt, S. S. 1994, *PASJ*, 46, L37
- Zdziarski, A. A., Johnson, W. N., & Magdziarz, P. 1996, *MNRAS*, 283, 193

Figure Captions

Figure 1

Panels (a)–(f) show results of *ASCA* simulations using models 1–6 respectively (see Table 1 and text). Shown are the distributions of $\Delta C_{\text{true}} \equiv C_{\text{true}} - C_{\text{min}}$ (stars) and $\Delta C_i \equiv C_i - C_{\text{min}}$ for each parameter i (the symbols explained in Figures 1a and 1b pertain to Figures 1c–1e too). The theoretical χ^2 probability distributions (solid curves) are shown for 1 degree of freedom (χ_1^2 ; uppermost curves) up to p degrees of freedom (χ_p^2 ; lowest curves), where p is the total number of free parameters in the model. In each case the ΔC_{true} distributions follow χ_p^2 and the ΔC_i all follow χ_1^2 , as they should.

Figure 2

Simulation results using model 3 (power law plus a narrow Gaussian emission line with the parameters shown in Table 1). Plots show $\Delta C_{\text{true}} \equiv C_{\text{true}} - C_{\text{min}}$ (dots) and $\Delta C_i \equiv C_i - C_{\text{min}}$ (crosses) versus the best-fitting values of the model parameters (N_H is in units of 10^{21} cm^{-2} ; line center energy, E_{Fe} , and line intrinsic width, σ_{Fe} are in units of keV; line intensity is in units of $10^{-4} \text{ photons cm}^{-2} \text{ s}^{-1}$; power-law normalization is in units of $\text{photons cm}^{-2} \text{ s}^{-1} \text{ keV}^{-1}$ at 1 keV; Γ is the power-law photon index).

Figure 3

The solid line shows the distribution of best-fitting emission-line equivalent width values from the simulations using model 3 (see §4). The dotted line shows the distribution of best-fitting emission-line intensity values from the same simulations, scaled by the input equivalent width (500 eV) for direct comparison. The two distributions are indistinguishable, so for real data, confidence regions for emission-line equivalent widths can be obtained from the confidence regions for the intensity, scaled by the best-fitting equivalent width.

Figure 4

Results of simulations using model 2 (absorbed power law plus a Gaussian emission line) with reduced exposure times of (a) 4 Ks, and (b) 400 s. The center energy and intrinsic width of the Gaussian emission-line component are held fixed at 6.4 keV and 0.1 keV respectively.

Figure 5

Results of simulations using model 2 (absorbed power law plus a Gaussian emission line) with exposure times of (a) 40 Ks, (b) 4 Ks, and (c) 400 s. Shown are the distributions of $\Delta C_{\text{true}} \equiv C_{\text{true}} - C_{\text{min}}$ (dots) and $\Delta C_i \equiv C_i - C_{\text{min}}$ (crosses) versus the best-fitting values of the emission-line intensity, I_{Fe} , in units of photons $\text{cm}^{-2} \text{s}^{-1}$.

Figure 6

Results of simulations using model 1 (simple absorbed power law only), in which the simulated spectra are fitted with an additional Gaussian emission line in the model. This simulates the case of obtaining confidence regions (upper limits) on the intensity or equivalent width of an emission line when the ‘true’ model has no emission line. The center energy and intrinsic width of the Gaussian emission-line component are held fixed at 6.4 keV and 0.1 keV respectively. See §6 for details.

TABLE 1: MODELS USED IN THE SIMULATIONS

Model	Description	Free Parameters
1	Power law plus absorption (photon index, $\Gamma = 1.7$, normalization = 1.226×10^{-2} photons $\text{cm}^{-2} \text{s}^{-1} \text{keV}^{-1}$ @ 1 keV, column density, $N_H = 5 \times 10^{21} \text{cm}^{-2}$).	3
2	As model 1, with the addition of a Gaussian line with center energy, $E_{\text{Fe}} = 6.4 \text{keV}$, equivalent width, $EW = 100 \text{eV}$ (intensity, $I_{\text{Fe}} = 5.2356 \times 10^{-5}$ photons $\text{cm}^{-2} \text{s}^{-1}$) and intrinsic width, $\sigma_{\text{Fe}} = 0.1 \text{keV}$ (FWHM $\sim 2.35\sigma_{\text{Fe}}$).	6
3	As model 2 except that $EW = 500 \text{eV}$.	6
4	As model 2 except that $\sigma_{\text{Fe}} = 0.3 \text{keV}$.	6
5	As model 2 except that $\sigma_{\text{Fe}} = 0.01 \text{keV}$.	6
6	Power law plus absorption (photon index, $\Gamma = 1.7$, normalization = 1.226×10^{-2} photons $\text{cm}^{-2} \text{s}^{-1} \text{keV}^{-1}$ @ 1 keV, $N_H = 5 \times 10^{21} \text{cm}^{-2}$) plus an absorption edge at 0.8 keV (fixed) with an optical depth at threshold, $\tau_0 = 0.2$.	4

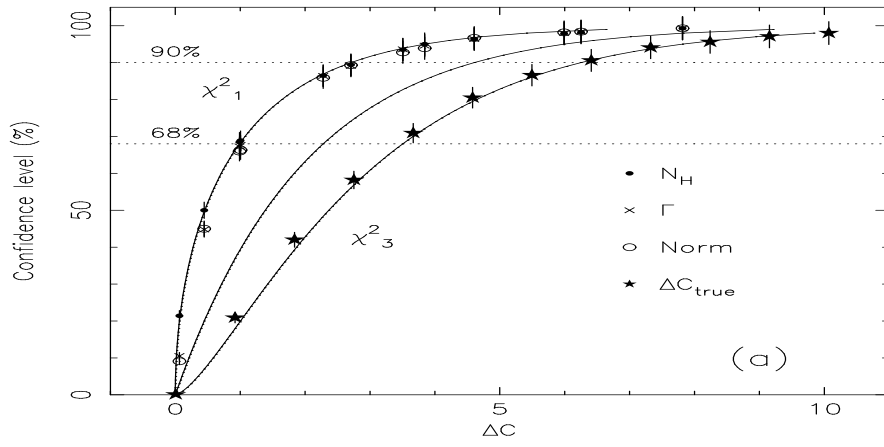


Figure 1(a)

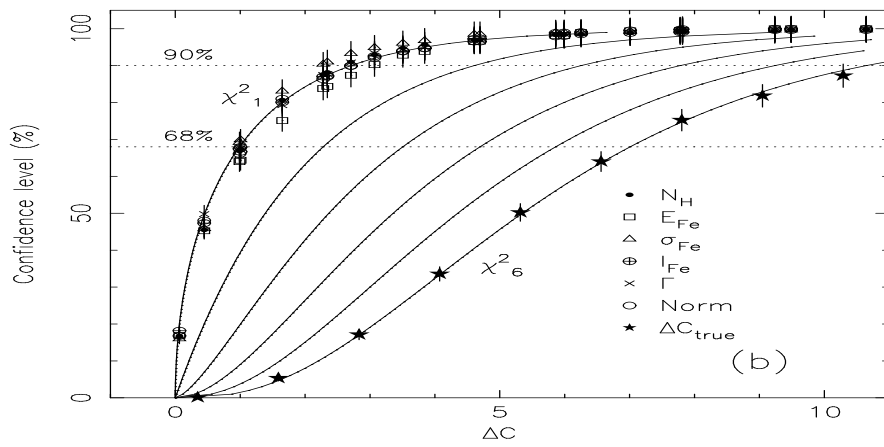


Figure 1(b)

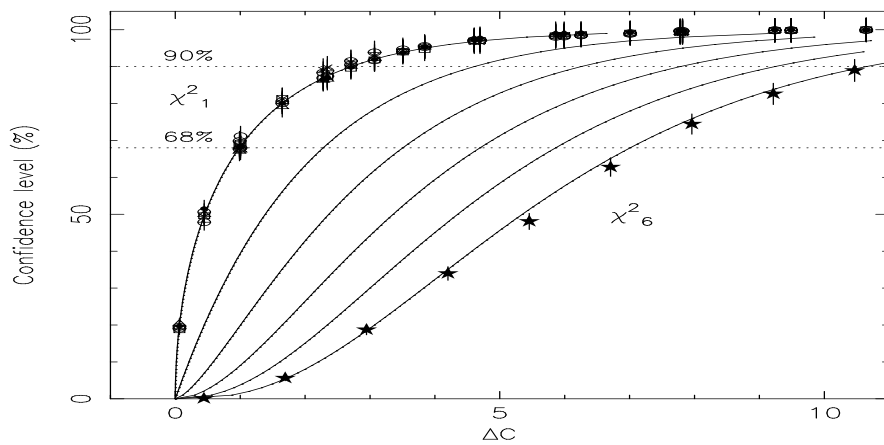


Figure 1(c)

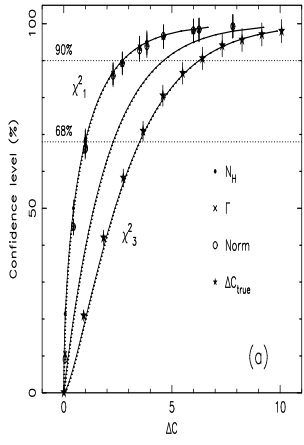


Figure 1(a)

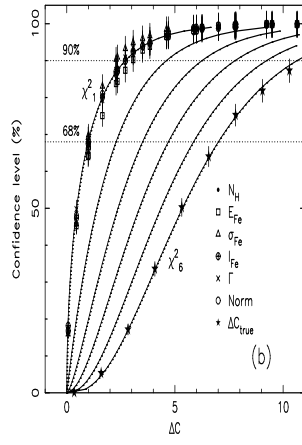


Figure 1(b)

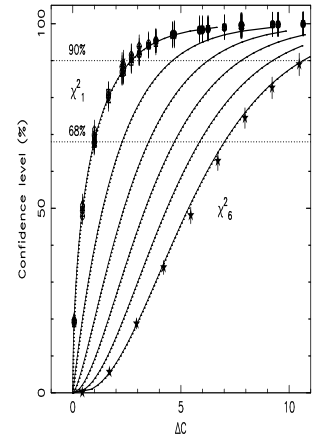


Figure 1(c)

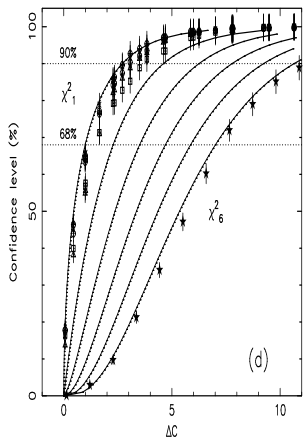


Figure 1(d)

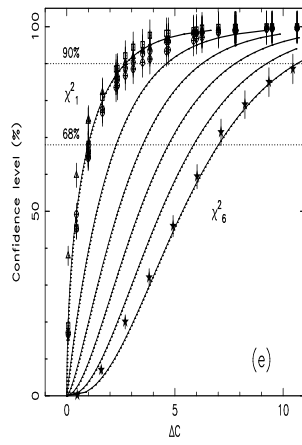


Figure 1(e)

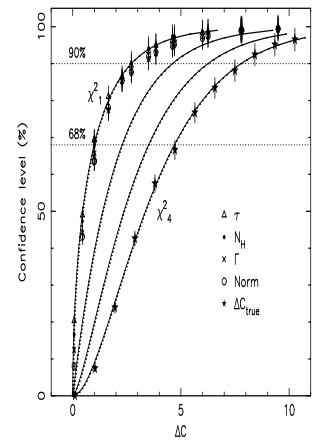
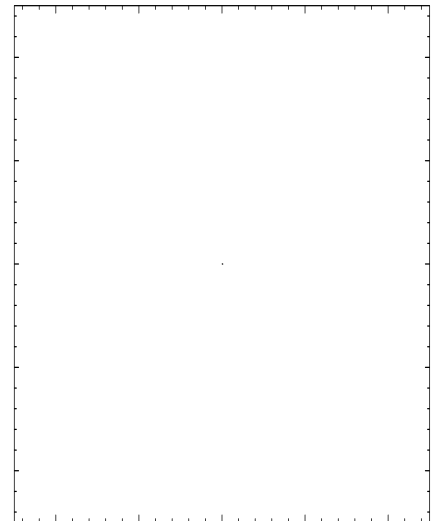
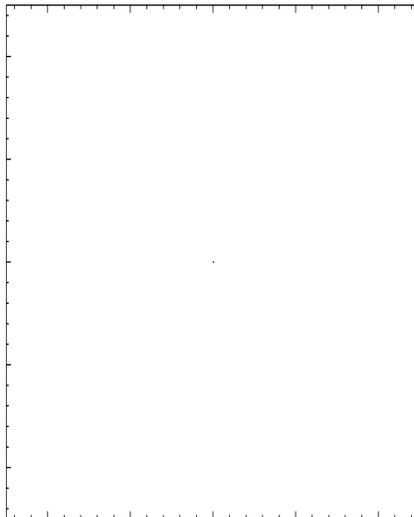
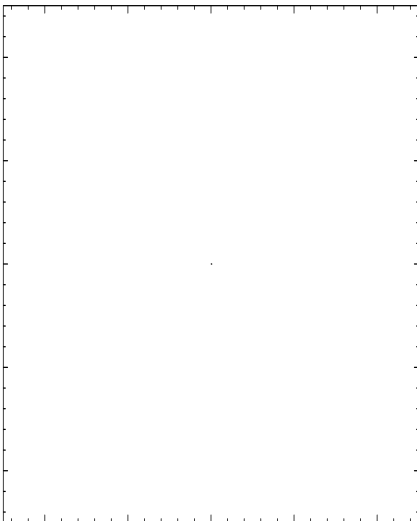


Figure 1(f)



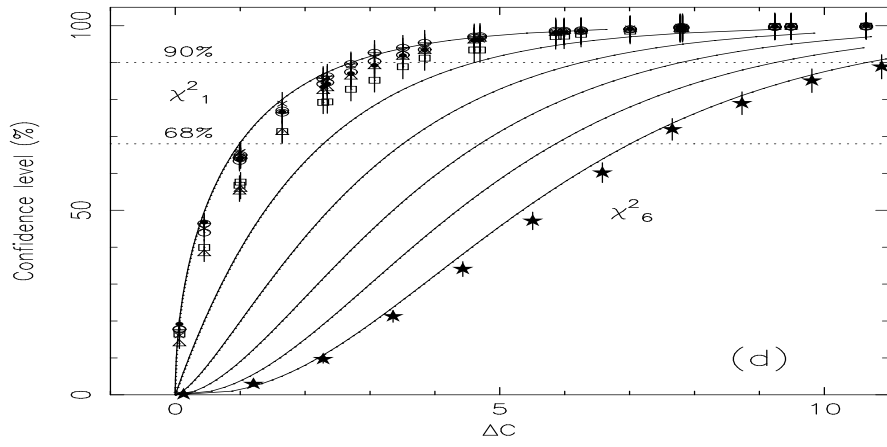


Figure 1(d)

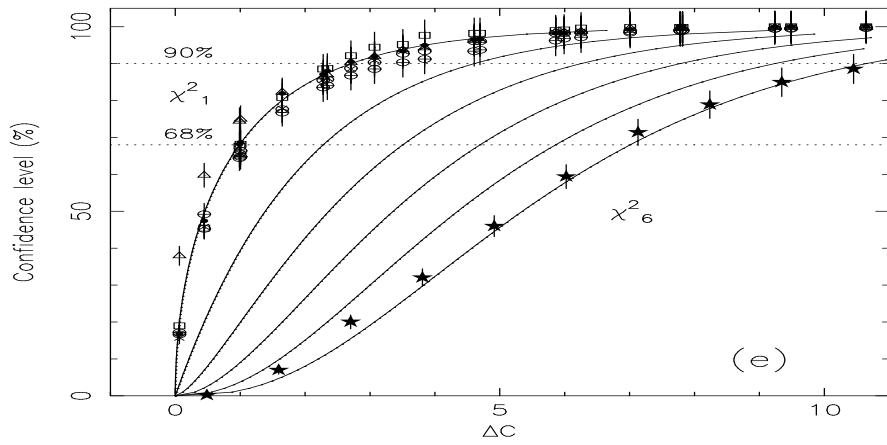


Figure 1(e)

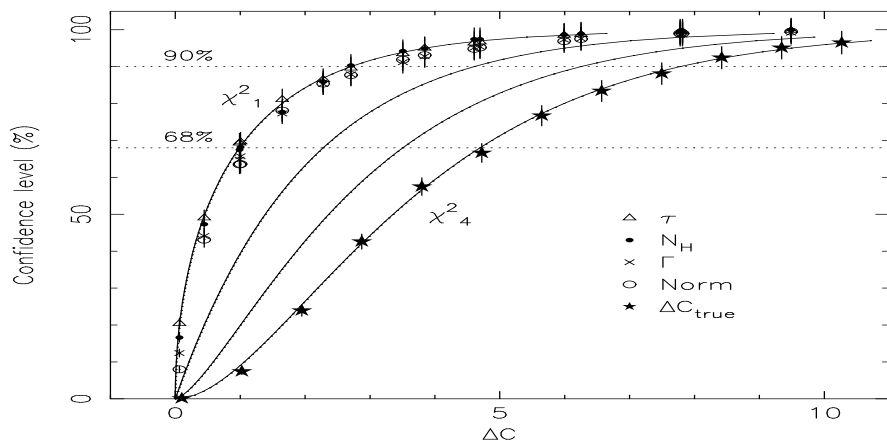


Figure 1(f)

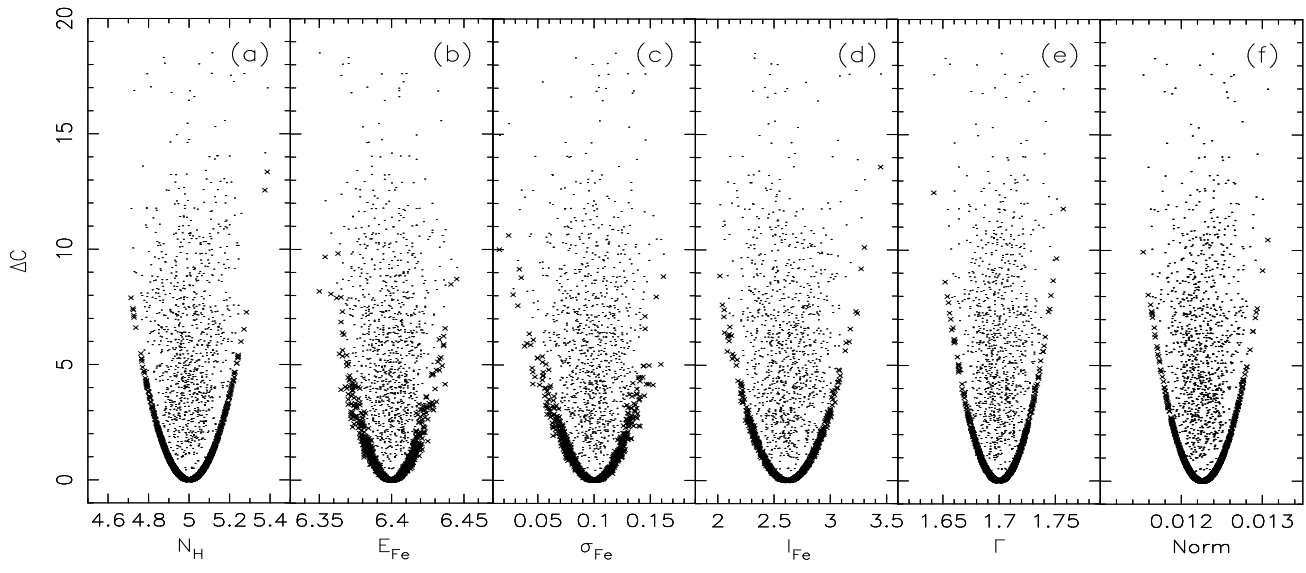


Figure 2

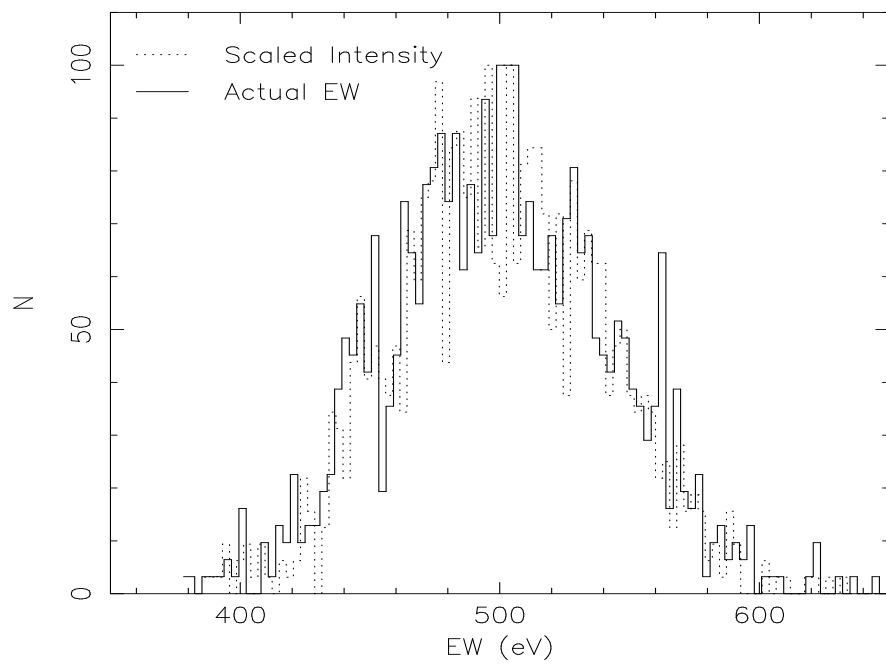


Figure 3

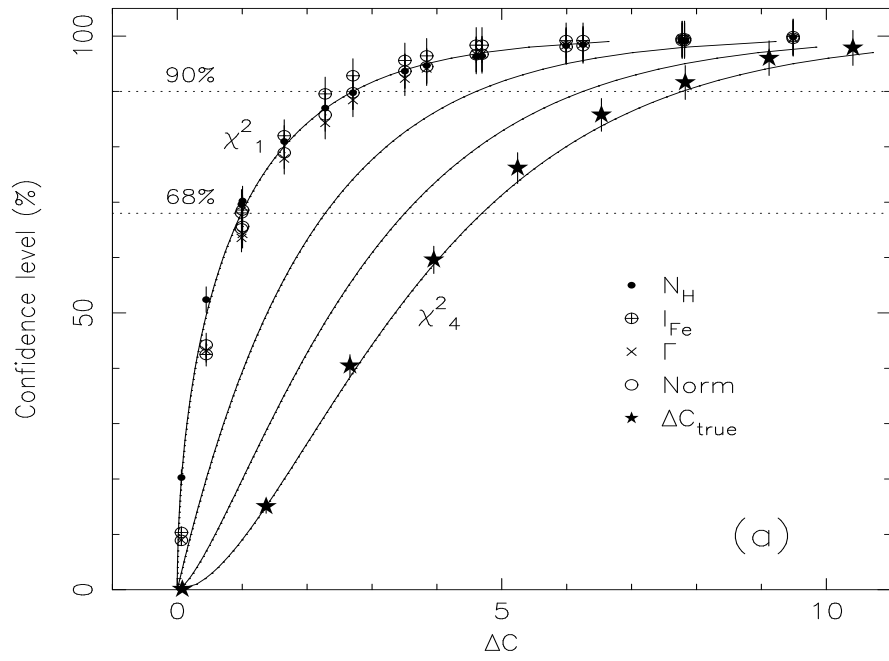


Figure 4(a)

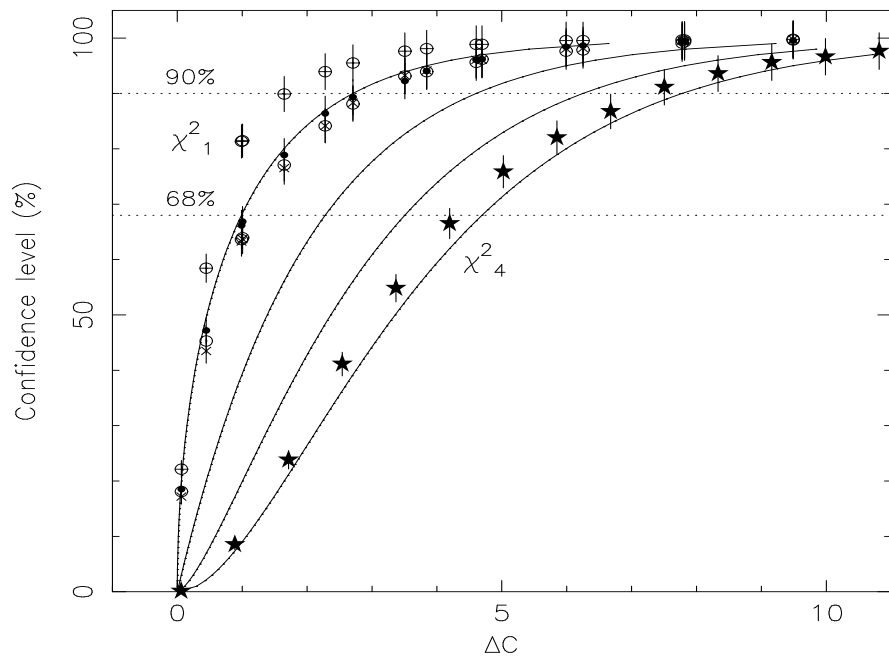


Figure 4(b)

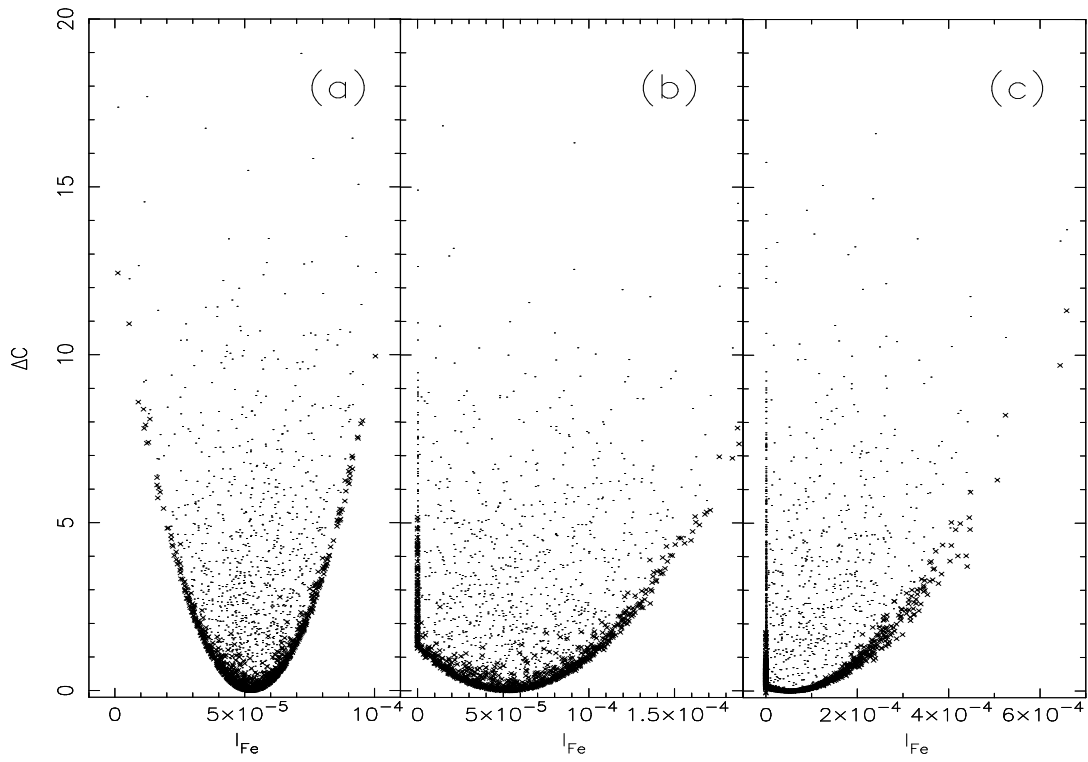


Figure 5

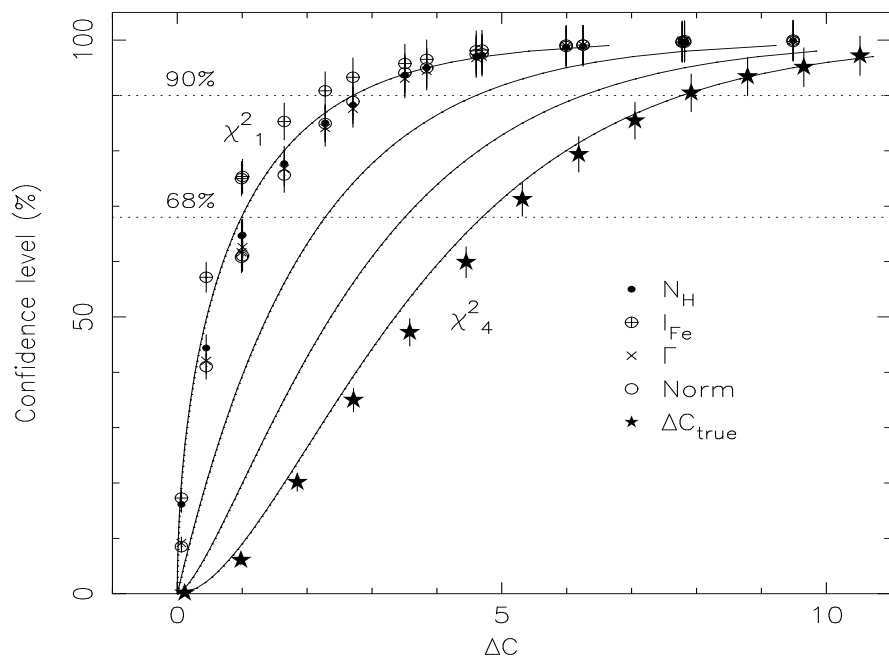


Figure 6